Systematic Evaluation of Fluorination as Modification for Peptide-Based Fusion Inhibitors against HIV-1 Infection

Susanne Huhmann,[a] Elisabeth K. Nyakatura,[a, b] Anette Rohrhofer,[c] Johann Moschner,[a] Barbara Schmidt,[c] Jutta Eichler,[d] Christian Roth,[e] and Beate Koksch*[a]

With the emergence of novel viruses, the development of new antivirals is more urgent than ever. A key step in human immunodeficiency virus type 1 (HIV-1) infection is six-helix bundle formation within the envelope protein subunit gp41. Selective disruption of bundle formation by peptides has been shown to be effective; however, these drugs, exemplified by T20, are prone to rapid clearance from the patient. The incorporation of non-natural amino acids is known to improve these pharmacokinetic properties. Here, we evaluate a peptide inhibitor in which a critical Ile residue is replaced by fluorinated analogues. We characterized the influence of the fluorinated analogues on the biophysical properties of the peptide. Furthermore, we show that the fluorinated peptides can block HIV-1 infection of target cells at nanomolar levels. These findings demonstrate that fluorinated amino acids are appropriate tools for the development of novel peptide therapeutics.

Introduction

Protein-protein interactions play an important role in several biological processes, for example, electron transfer, cell signaling and cell invasion. Thus, their selective disruption has emerged as an excellent strategy for drug discovery. Viruses dock and fuse with host cells using protein-mediated fusion events. In human immunodeficiency virus (HIV) infection, which causes the acquired immunodeficiency syndrome (AIDS), the virus's envelope glycoprotein subunit gp41 mediates membrane fusion between the virus and host cell. A crucial step in this process involves a helix-helix interaction between the *N*- and *C*-terminal heptad repeats (CHR and NHR) of gp41 that results in the formation of a coiled-coil six-helix bundle (6-HB). In this structure, three CHR-helices pack in antiparallel fashion around the outside of a central coiled-coil trimer formed by three NHR-helices. This event brings the viral and the host cell membranes into close proximity and induces cell fusion.[1] During 6-HB assembly a pre-hairpin intermediate that bridges the viral and target cell membranes is formed. In this intermediate state, which has a relatively long lifetime of several minutes, the NHR- and CHR regions are spatially separated. This provides a therapeutic opportunity in which synthetic peptides derived from either CHR or NHR can competitively bind to their respective counterpart regions, thereby preventing the conversion of gp41 to its fusion active conformation and inhibiting HIV-1 infection.[2]

An approved peptidogenic antiviral drug is T20 (Enfuvirtide, Fuzeon), a 36 amino acid peptide, the first and currently only HIV-1 fusion inhibitor in clinical use. Its low toxicity and high target specificity make it a highly potent antiviral drug. However, T20 shows rapid *in vivo* proteolysis, poor oral bioavailability, and an early resistance onset is observed. For these reasons, frequent high dosage administration by subcutaneous injection is required, thus T20 is administered only when other antiretroviral drugs are ineffective.[3] The lessons taught by T20 are in many ways broadly representative for the field of peptide-based therapeutics: they tend to be plagued by poor pharmacokinetics but also tend to possess unparalleled efficacy.[4] Viral fusion inhibitors offer many advantages, making the development of next-generation T20-like therapeutics of great interest. First, this class of compounds acts outside of the cell and targets exclusively proteins of the virus, contributing to the usually low drug-related toxicity compared to drugs that target the intracellular lifecycle of the virus or act on host cellular proteins.[1b] Moreover, targeting the virus before it invades host cells might lead to a prophylactic effect, similar to vaccine-induced immunity.[5] Over the last years, several concepts and strategies have been reported to improve peptidogenic fusion inhibitors[2b–d,5–6] including designed salt-bridges,[3b,7] the introduction of D-amino acids,[8] backbone

[a] Dr. S. Huhmann, Dr. E. K. Nyakatura, Dr. J. Moschner, Prof. Dr. B. Koksch
Freie Universität Berlin,
Department of Biology, Chemistry and Pharmacy,
Institute of Chemistry and Biochemistry
Arnimallee 20, 14195 Berlin (Germany)
E-mail: beate.koksch@fu-berlin.de
[b] Dr. E. K. Nyakatura
Antibody Engineering Tri-Institutional Therapeutics Discovery Institute
417 East 68th Street, 19 Floor North, P: 646-888-2003, New York, NY 10021 (USA)
[c] A. Rohrhofer, Prof. Dr. B. Schmidt
Institute of Clinical Microbiology and Hygiene,
Regensburg University Hospital
Franz-Josef-Strauß-Allee 11, 93053 Regensburg (Germany)
[d] Prof. Dr. J. Eichler
Friedrich-Alexander-Universität Erlangen-Nürnberg,
Department Chemie und Pharmazie
Nikolaus-Fiebiger-Str. 10, 91058 Erlangen (Germany)
[e] Dr. C. Roth
Max Planck Institute of Colloids and Interfaces,
Biomolecular Systems, Arnimallee 22, 14195 Berlin (Germany)

Supporting information for this article is available on the WWW under https://doi.org/10.1002/cbic.202100417

crosslinks,[9] hydrogen-bond-surrogates,[10] foldamers,[11] cyclization,[12] multimerization,[13] conjugation to small molecules[14] or different classes of lipids,[15] as well as PEGylation[16] or dual-targeting inhibitors.[17] The obtained derivatives showed antiviral activity at micro- to picomolar ranges with considerably improved metabolic stability compared to wildtype peptides.

The decoration of organic molecules with fluorine substituents is a widely used strategy to improve small molecule drugs, owing to fluorine's capacity to productively affect molecular properties such as conformation, pK_a values of neighboring functional groups, and hydrophobicity. Often, this leads to improved interactions with proteins, enzymes, receptors or membranes, thereby improving pharmacological properties, bioavailability and -activity.[18] Moreover, due to the remarkable stability of the fluorine covalent bond, these molecules often show improved metabolic stability.

With the advent of easy to access fluorine-containing amino acids,[19] these building blocks sparked a renewed interest for drug design[20] and peptide and protein engineering. Selective introduction of fluorine-containing amino acids into peptides can modulate distinct pharmacokinetic and physicochemical functionalities of the resulting biopolymers, including structure, folding or stability towards thermal and chemical denaturation. Furthermore, it can improve metabolic stability, biological activity, and bioavailability of peptide-based drugs.[21]

However, studies in model systems have shown that the influence of fluorination depends highly upon the precise nature of the fluorinated group, as well as its position in the sequence and/or microenvironment. We sought to introduce fluorinated amino acid analogues into a compound that targets the clinically relevant HIV-1 gp41 system to improve its properties. We designed a CHR-derived peptide and incorporated side-chain fluorinated amino acids that differ in size and fluorine content at a central and highly conserved interaction site to explore whether fluorine-specific interactions can improve the binding, stability and activity of the peptide as an HIV fusion inhibitor.

Results and Discussion

Design of fusion inhibitor C31

Nearly all peptide fusion inhibitors against HIV reported to date are derived from the CHR-region of HIV-1 gp41 (residues 628–673), with the C34 peptide sequence (amino acids 628–661 of CHR) as design template.[2b,c,6] NHR-derived sequences have also been investigated, but CHR-derived peptides usually show higher anti-HIV activity, partly attributable to the tendency of the former to aggregate.[22] One drawback of the current inhibitors is their large size, comprising 10 α-helical turns ($\geq$34-mer), which is the case because shorter peptides and small molecules have been shown to have low potency. This is largely attributed to the rather shallow, hard to target, binding cleft of the NHR trimer.[2c,6,23]

In this study, we designed a 31-residue, CHR-derived peptide denoted C31, based on the functional domains of the CHR/NHR region of HIV-1 gp41 (see Figure 1A). C31 contains the NHR pocket-binding domain (PBD; amino acids 628–635; blue in Figure 1A) that binds to the pocket-forming region in NHR (amino acids 565–581, red in Figure 1A). The PBD is important for the inhibitory activity of CHR-derived peptides as the interaction between the PBD and the pocket seems to be critical for 6-HB stabilization and virus-cell fusion.[24] Within the PBD-pocket interaction is also a salt bridge between Lys574 of NHR and Asp632 of CHR that further contributes to stability and is crucial for viral entry as well as inhibition.[25] Upstream of and immediately adjacent to the PBD is the motif ^{621}QIWNNMT^{627} (orange in Figure 1A), which was incorporated into C31 due to its importance for the stability of the gp41 6-HB core structure. CHR-derived peptides containing this motif show high thermal stability and nanomolar anti-HIV activity, even against T20- and C34-resistant variants.[26] This is partially attributed to a unique hook-like structure, adopted by Met626 and Thr627, often referred to as the M–T hook.[27] The M–T hook is thought to enhance binding affinity and antiviral activity of CHR-based peptide inhibitors, especially for short peptides that are otherwise inactive.[2d,28] We avoided the CHR sequence downstream of residue 650 in peptide C31, so as to bypass molecular recognition of the ^{547}GIV^{549} binding sequence in NHR (purple in Figure 1A), known to be a hotspot for resistance development.[29]

We chose Ile635 as the replacement site for the fluorinated aliphatic amino acids difluoroethylglycine (DfeGly), 5,5,5-trifluoroisoleucine (5^3-F_3Ile) and 5,5,5,5′,5′,5′-hexafluoroleucine (5^3,$5'^3$-F_6Leu) (see green star and chemical structures in Figure 1C). This Ile residue is located in the center of the C31 peptide sequence and is, together with Trp631 and Trp628, a highly conserved sequence motif (WWI-motif) in many viral strains, crucial for hydrophobic core formation with NHR.[24b] Particularly, the central Trp631 in conjunction with Ile635 seems to be important for gp41 affinity and viral activity.[24b] Especially several CH-π interactions are thought to contribute to the helix bundle stabilization. Therefore, the fluorinated amino acids were chosen as they all bear a γ-hydrogen atom that can engage in a possible intramolecular CH-π interaction between Ile635 and Trp631(Figure 1C). Introduction of highly, but not fully fluorinated residues can strengthen CH-π interactions due to the polarization of adjacent CH-bonds upon fluorination leading to enhanced protein stability.[30] With improving the CH-π interaction upon introduction of the different fluorinated amino acids here, we sought to stabilize and enhance the α-helical peptide structure, possibly leading to improved antiviral potency of the fusion inhibitors by increasing the affinity to the NHR trimer as proposed before.[7a,31]

Interaction of C31 peptides with NHR

C31 variants as well as the NHR-derived counterpart T21 (Figure 1A) were synthesized by solid-phase peptide synthesis using pseudoproline dipeptide building blocks to avoid on-resin

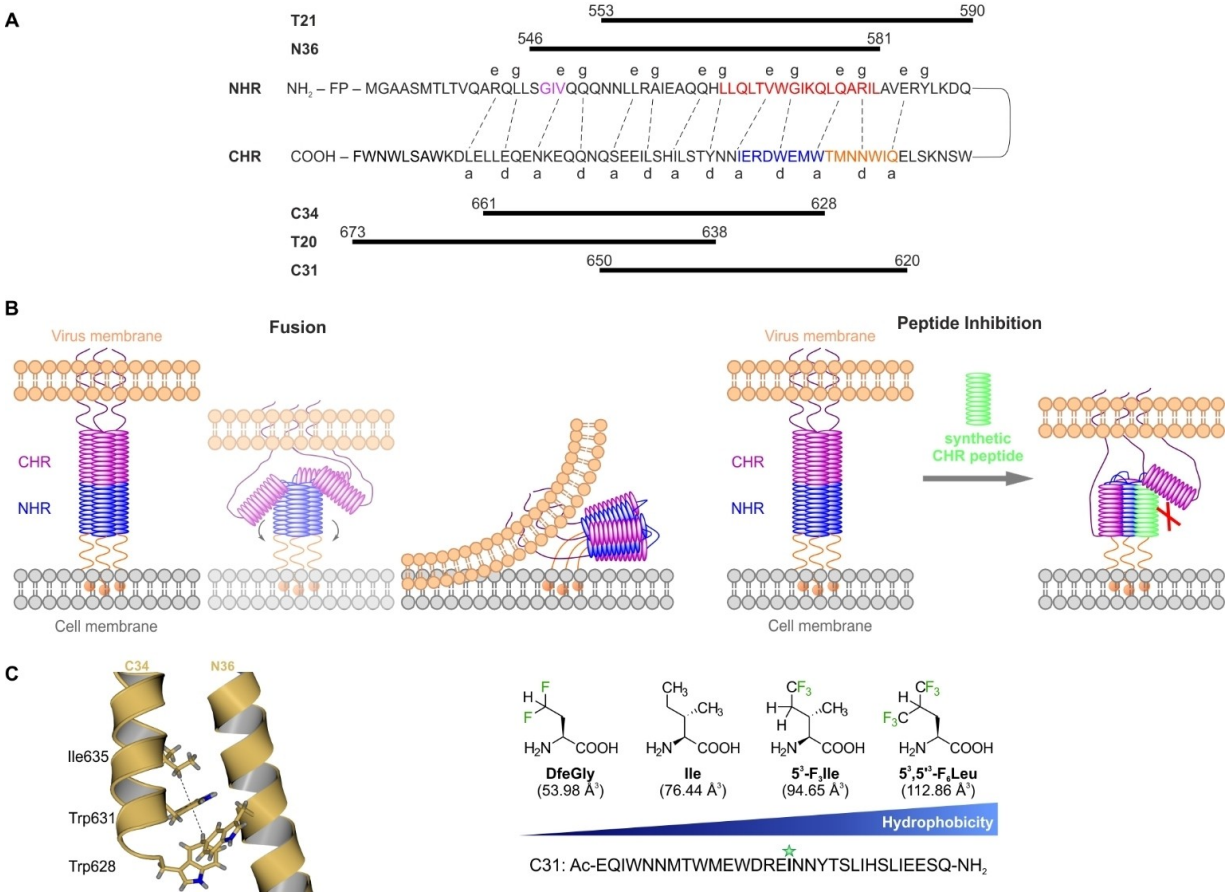

Figure 1. Rationale of the study. A) Sequence and interaction of the CHR- and NHR-region of gp41. Heptad repeats are shown in black. Dashed lines between the NHR- and CHR-regions indicate the interaction between the residues located at the **e**-, **g**- and **a**-, **d**-positions in NHR and CHR, respectively. Interaction of the pocket-binding domain (PBD, in blue) of the CHR with the pocket-forming domain (in red) of the NHR is critical for 6-HB formation. The region immediately adjacent to the PBD (in orange) is important for stabilization of the gp41 core structure. This motif may interact with the residues in the pocket-forming domain in the NHR and the downstream motif (AVERY). Peptide sequences derived from the NHR- or CHR-regions are shown above or below the sequence, respectively. B) Schematic representation of the HIV-1 viral fusion mechanism and inhibition of cell fusion. Synthetic peptides (green) derived from the CHR-region of gp41 can inhibit the formation of the fusion active conformation, and thus HIV infection, by interaction with their counterparts in gp41. C) Section of C34/N36 crystal structure (PDB code: 1AIK) showing the highly conserved WWI motif. Structures of fluorinated amino acids used to replace Ile635 of C31. The side chain vdW volumes (starting at Cβ) given in parentheses were calculated according to Zhao *et al.*[34] C31 sequence, derived from residues 620–650 of gp41.

aggregation (for detailed synthetic procedures see Supporting Information). To assess the secondary structure and the formation of the 6-HB with our peptides, we used CD spectroscopy. The CD experiments reveal that, while being unstructured by itself, all C31 peptides form α-helical bundles with T21 as evidenced by the two distinct minima observed (Figure 2A). The substitution of Ile635 by the different fluorinated amino acids causes no significant structural perturbation. In fact, the fluorinated bundles appear to have slightly higher helical contents compared to the parent C31/T21 complex (72–73% vs. 68%), despite fluorinated amino acids tend to have lower α-helix propensities.[32] This is in line with previous experiments, showing that the destabilizing effect of fluorine is often compensated by the overall tendency of proteins to form stable tertiary structures.[33]

Next, we determined the thermal stability of the complexes by monitoring changes in the CD signal at 222 nm over increasing temperatures from 25 to 100 °C (Figure 2B). The helix bundles containing either DfeGly, 5^3-F_3Ile or 5^3,$5'^3$-F_6Leu exhibit slightly reduced melting temperatures compared to the non-fluorinated C31/T21 complex (72.5 °C, 73.6 °C and 68.5 °C, respectively, versus 77.2 °C). However, no clear trend could be observed. The greater hydrophobicity of the organofluorine groups should favor bundle formation and therefore stability, but the polarization of the C–F bond and the steric demand, in particular of 5^3,$5'^3$-F_6Leu, might counteract that effect. In case of DfeGly, the more hydrophilic character compared to Ile[32c] may be a reason for the lower thermal stability observed.

To determine whether fluorination influences the oligomeric state of the C31/T21 complex, SEC/MALS measurements were performed. Three of the tested peptide combinations showed the expected molecular weight for a 6-HB (Figure 2C, Table 1, and Supporting Information Figure S6). On the contrary, for the C31-DfeGly/T21 complex no reliable data could be obtained. Likely, aggregation of the fluorinated peptide prior mixing prevented the formation of the 6-HB complex and only the T21

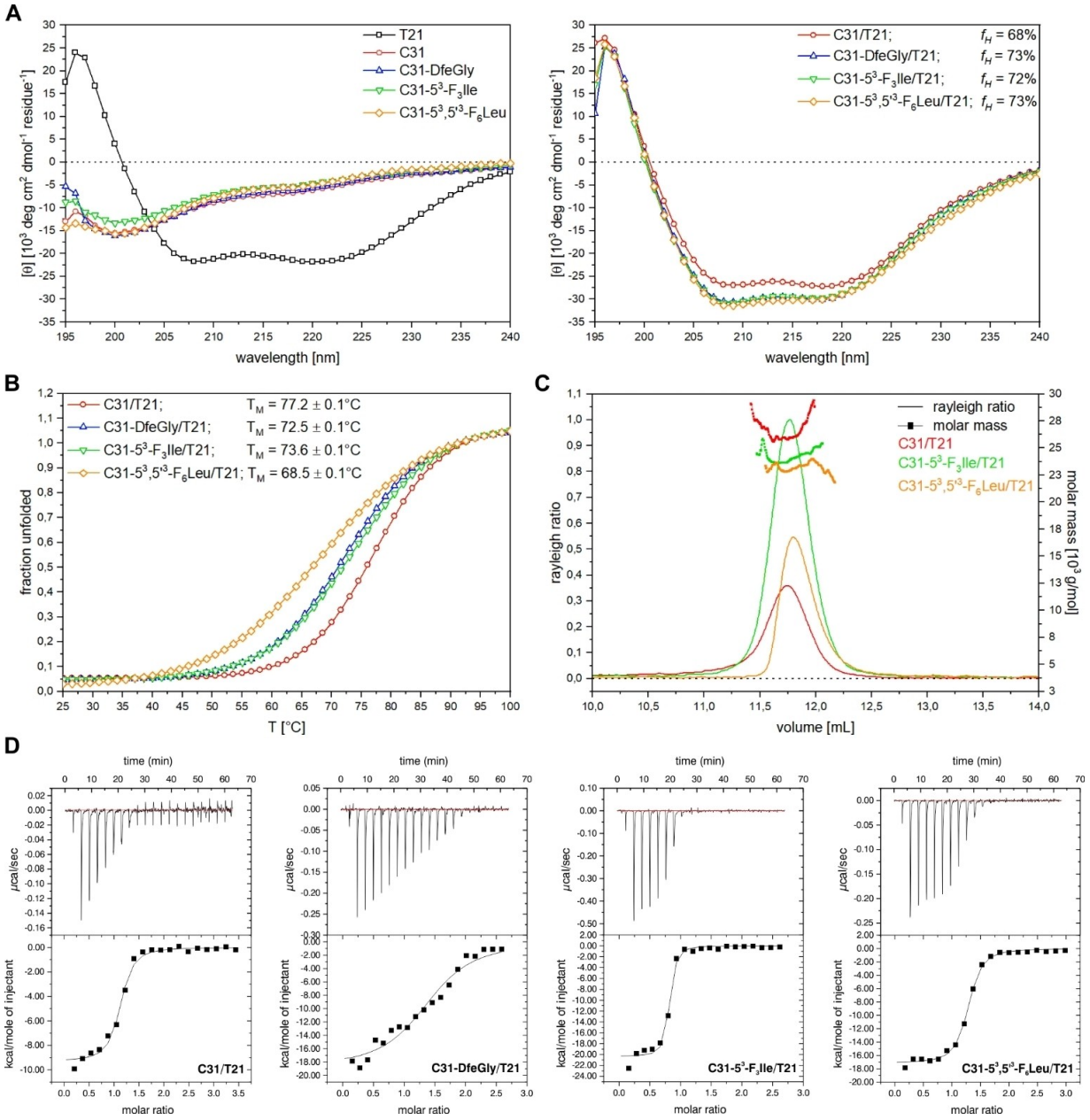

Figure 2. Structural and thermodynamic characterization of complex assembly. A) CD spectra of the C31 peptides and T21 alone (left panel) and in equimolar mixture (right panel). Helical content (f_H) for each mixture given in the legend. B) Fitted thermal denaturation curves of equimolar mixtures of C31 peptides with T21. Melting point (T_M) for each given in the legend. C) Molecular mass estimation of C31/T21 assemblies by SEC/MALS. D) ITC assay of C31 peptides with T21. The upper panels show the heat flows (power) resulting from each injection plotted against time. The bottom panels show the normalized integration data of each spike in the upper panel plotted against molar ratio, yielding heat (enthalpy) exchanged after each injection.

Table 1. Theoretically and experimentally determined molecular weights of C31/T21 complexes.

	SEC/MALS determined mass [Da]	Theoretical 6-HB mass [Da]
C31/T21	26480 ± 490	25420
C31-5³-F_3Ile/T21	24140 ± 409	25591
C31-5³,5'³-F_6Leu/T21	23190 ± 314	25744

peptide eluted as monomer in a single peak in the SEC/MALS experiment (Supporting Information, Figure S6).

The thermodynamic parameters for binding of the different C31 peptides to T21 were investigated by ITC (Figure 2D, Table 2). As indicated by the negative peaks in the ITC graph (Figure 2D, upper panels), all C31 peptides bind in an exothermic fashion to the T21 peptide. As expected for a 1:1 binding stoichiometry, the number of binding sites N between C31 and T21 was found to be 1.07 (Table 2). Binding of C31-DfeGly and C31-5³,5'³-F_6Leu to T21 gave higher stoichiometries of 1.43 and 1.23, respectively. In contrast, for C31-5³-F_3Ile a reduced stoichiometry with a value of 0.76 was determined.

Table 2. Kinetic parameters obtained for binding of C31 peptides to T21 from ITC measurements.

	N [sites]	K [10^6 M^{-1}]	ΔH [kcal mol^{-1}]	ΔS [cal mol^{-1} deg^{-1}]	ΔG kcal mol^{-1}]
C31/T21	1.07 ± 0.02	9.4 ± 2.3	−9.3 ± 0.2	0.72	−9.5
C31-DfeGly/T21	1.43 ± 0.05	1.2 ± 0.3	−18.8 ± 0.9	−35.2	−8.3
C31-5^3-F_3Ile/T21	0.76 ± 0.01	22.3 ± 7.9	−20.3 ± 0.4	−34.5	−10
C31-5^3,$5'^3$-F_6Leu/T21	1.23 ± 0.01	13.5 ± 1.7	−17.2 ± 0.2	−25.0	−9.8

This might be due to inaccuracies in peptide concentrations, as a result of partial aggregation of the fluorinated peptides over the time course of the experiment. All variants show comparable binding constants (Table 2) except C31-DfeGly. The formation of the helical assembly of the C31 peptides with T21 is an enthalpy-driven reaction, in which a large amount of heat is released, especially for the fluorinated derivatives. This is in line with the increased number of close contacts formed with the fluorinated peptides compared to the wildtype, as observed in the X-ray structures described below. The formation of the 6-HB leads in case of the fluorinated variants to unfavorable entropic contributions, likely because the fluorinated side chains maximally occupy the binding pocket as demonstrated by the X-ray structures resulting in less degrees of freedom of the fluoro-modified peptide once it is bound to T21. Furthermore, reduced solvent fluctuations within the pocket may contribute to the large enthalpic gain and the relatively large entropic penalty contrary to the classic model of the hydrophobic effect.[35]

Inhibitory activity of C31 peptides

To test whether fluorination of selected positions of C31 affects its HIV-1 inhibitory activity, an infection assay was performed (Figure 3). We found that all peptides can inhibit infection of CEMx174 reporter cells with IC_{50} values ranging from nano- to low micromolar range. Whereas DfeGly and 5^3-F_3Ile show similar values to the wildtype, 5^3,$5'^3$-F_6Leu lead to a 56-fold loss in activity (IC_{50} value of 1.49 μM versus 26.5 nM). This might be a result of the steric repulsion of 5^3,$5'^3$-F_6Leu compared to the other fluorinated analogues. This may also be reflected in the lower stability of the complex, revealed by the thermal denaturation assays. Nevertheless, the other variants have activities comparable to the clinically used T20 (IC_{50} = 24–36 nM).[15b,36] Despite binding more weakly to T21 and not forming a stable 6-HB in SEC/MALS, the similar IC_{50} value of C31-DfeGly compared to the parent C31 peptide is likely attributable to the experimental set-up using lower concentrations, so that aggregation does not occur here. Furthermore, different or multiple interaction sites within the viral fusion apparatus might be possible as proposed for the fusion inhibitor T20 before.[37]

Crystal structure of 6-HB complexes

To compare the interactions of the fluorinated variants with the wildtype, we aimed to crystallize all four variants of the 6-HB. We obtained structures for the wildtype, as well as the DfeGly and 5^3-F_3Ile containing analogues to high resolution (Supporting Information, Table S9). No suitable crystals could be obtained for the 5^3,$5'^3$-F_6Leu complex. All variants crystallized in the space group H32 with one T21 and one C31 peptide in the asymmetric unit (Figure 4A). Clear electron density allowed the unambiguous identification of the fluorinated amino acids (Supporting Information, Figure S8). An analysis of the likely oligomeric state using PISA[38] confirmed that all three variants form the expected 6-HB (Figure 4B and C).

Of particular interest was the interaction of the fluorinated analogues within the conserved NHR pocket, known to be important for the formation of the complex and therefore, antiviral activity. In all three structures, the side chains lining the pocket are invariant in their position, indicative that the pocket can tolerate larger substitutions. However, with increasing fluorine content the number of close contacts within 4 Å increases from two to seven (Table 3).

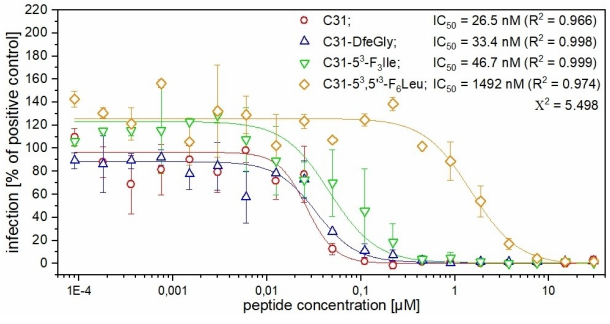

Figure 3. Antiviral activity of C31 peptides. Inhibition of infection of CEMx174 SEAP cells with HIV-1_{NL4-3} by C31 peptide and fluorinated variants.

Table 3. Intra- and intermolecular mean distances between Ile635 or fluorinated residues of C31 and interacting partners in T21 or C31 within 4 Å based on the X-ray crystal structures.

Residue	C31-Ile635 [Å]	C31-DfeGly635 [Å]	C31-5^3-F_3Ile635 [Å]
T21-Leu565	3.66	2.98	3.11
			3.28
T21-Leu568	3.93	3.45	3.24
		3.59	3.33
T21-Thr569			3.76
T21-Val570		3.46	
		3.71	
C31-Trp631		3.17	3.12
			3.18

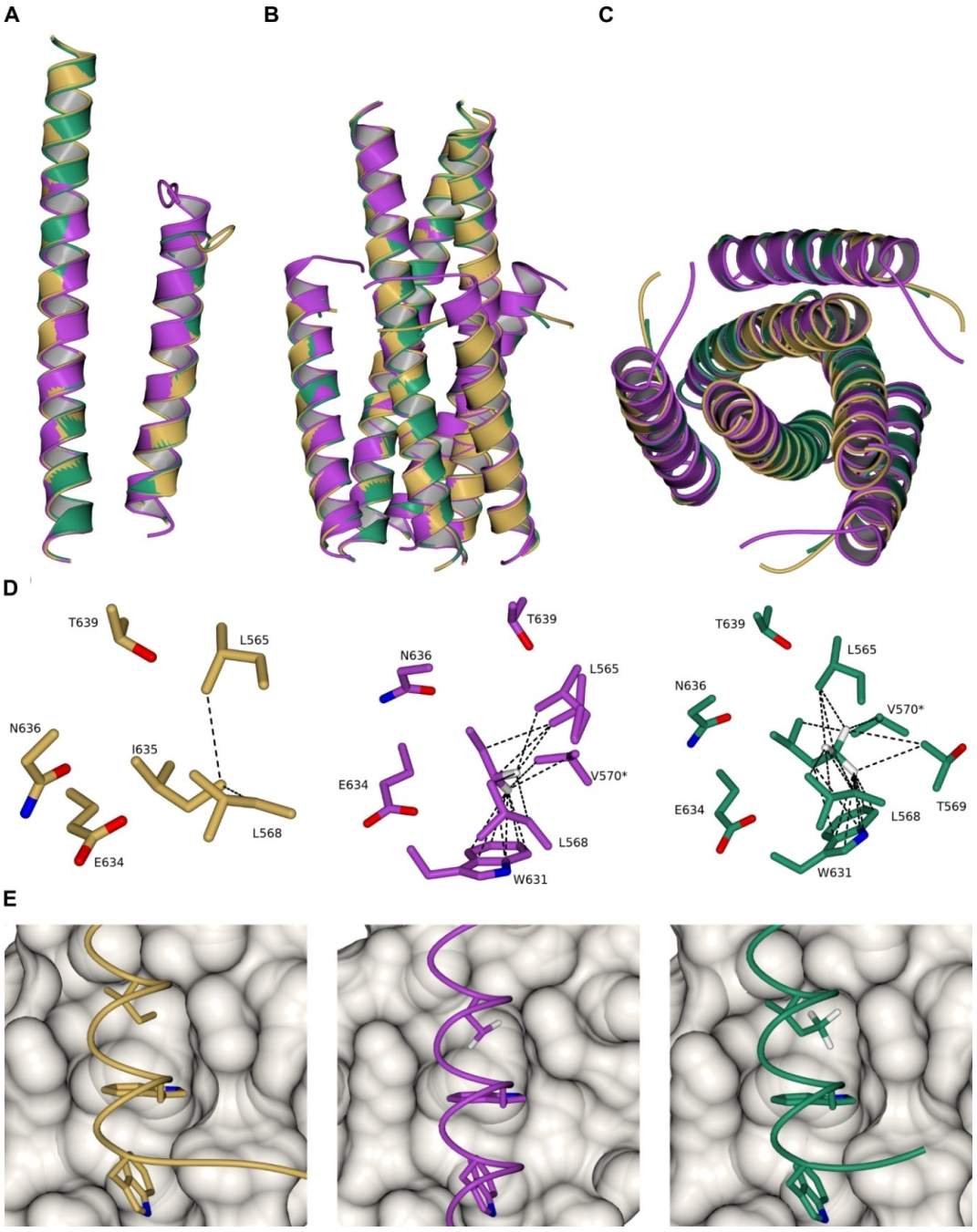

Figure 4. Crystal structure analysis of C31/T21 complexes. Structure of wildtype C31/T21 (sand), C31-DfeGly/T21 (purple) and C31-5^3-F_3Ile/T21 (green) in ribbon representation and interaction pattern of Ile635 in the targeted pocket of the T21 trimer. A) Overlay of the content of the asymmetric unit of each variant T21 is the longer helix, whereas C31 represents the shorter helix. All three structures overlay with a maximum r.m.s.d. of 0.3 Å. B) Oligomeric assembly of the stable 6-HB. C) Top view of the helical bundle. T21 forms the inner trimer and is surrounded by the C31 helices. D) Interacting residues around Ile635 and variants thereof in stick representation, with the contacts <4 Å shown as dashed lines. Residues marked with a star are part of a second NHR helix, not part of the asymmetric unit. E) The pocket filling residues Trp628, Trp631 and Ile635 and variants thereof in stick representation in the hydrophobic pocket of the T21 trimer, shown as surface in gray.

Furthermore, the targeted pocket volume is neatly filled by 5^3-F_3Ile. Larger substituents, like 5^3,$5'^3$-F_6Leu, most likely lead to steric clashes with the pocket lining residues (Figure 4D, E). This would explain the lower thermal stability, as well as the impaired HIV-1-inhibitory activity of that peptide variant. In earlier studies the *N*-terminus of the CHR helix, in particular Met626 and Thr627 have been identified to be important for antiviral activity.[28a] This was attributed to an unusual side-chain hydrogen bond of Thr627, which disrupts the helix and changes the direction of the *N*-terminus. We wondered if the fluorinated residue might also stabilize the M–T hook by remote participation via Trp631. We observed in two of our structures a

similar conformation with Met626 taking part in a hydrophobic cluster with Trp628, Trp631 and Trp571 (Supporting Information, Figure S8). However, we observed an alternative conformation in the variant with DfeGly, whereby the helix is extended by approximately one turn, positioning Met626 on the opposite site. Now, Trp623 takes the approximate position of Met626 in the hydrophobic pocket. An even more extended helical arrangement is seen in a structure solved by Yao *et al.*[39] That points towards a considerable flexibility of the *N*-terminal part of CHR, with the M–T hook playing a minor role and may only help to transiently stabilize the hydrophobic core, assisting the 6-HB formation before it is resolved and the CHR helix is fully formed in the final fusion complex.

Conclusion

Viral infections are a major threat to human health, due to the lack of antiviral drugs. The high mutagenic rate and the use of the host's own replication machinery make it hard to develop new efficient antiviral drugs. Peptide-based viral fusion inhibitors are attractive compounds to inhibit viral entry, but often suffer from low bioavailability and stability. In small molecule drugs, fluorination is an attractive modification to overcome such shortcomings. We sought to transfer that concept in the field of peptide therapeutics using fluorinated amino acids. We generated a series of HIV fusion inhibitor peptides with fluorinated amino acids in a key position of a conserved sequence motif, essential for activity and performed a structural characterization and biophysical analysis of these peptides. We could show that fluorinated analogues are generally well tolerated and prove for a small family of fluorinated C31 derivatives that one can modulate specifically the peptide-peptide interaction. Even small changes have profound consequences on the stability of the 6-HB. In particular, the optimal size of the fluoro-substituted residue seems important when surface pockets or clefts are targeted. Our structural data show that C31-5^3-F_3Ile has the optimal size to fill the targeted PBD-pocket without steric repulsion, which would interfere with the stability and therefore inhibitory potential of the peptide. Despite having higher helicity for all and increased binding affinity for some of the fluorinated peptides, the inhibitory activity is not improved compared to the parent C31. Therefore, we are currently working on a second generation of fluorinated peptide-based inhibitors that, if they show improved potencies, will also be tested for proteolytic stability. Nevertheless, our results open up new opportunities and directions for the development of novel peptide-based fusion inhibitors with non-natural building blocks, probably also for other viruses relying on helical bundle formation for cell fusion. Examples include paramyxoviruses (e.g. human respiratory syncytial virus (HRSV)), orthomyxoviruses (e.g. influenza virus), filoviruses (e.g. Ebola, Marburg), coronaviruses (e.g. severe acute respiratory syndrome (SARS)), and other retroviruses (e.g. human T-cell lymphotropic virus). Furthermore, the use of fluorinated amino acids is a promising approach to target and influence protein-protein interactions, an emerging field in drug development.

Experimental Section

Peptide synthesis, purification, and characterization: Peptide synthesis occurred at a 0.05 mmol scale by standard Fmoc/^{t}Bu protecting group strategy[40] using an Activo-P11 Automated Peptide Synthesizer (Activotec) and is described in detail in the Supporting Information. Peptides were cleaved from the solid support by treatment with trifluoroacetic acid (TFA) containing 5% (v/v) thioanisol, 2.5% (v/v) 1,2-ethanedithiol, 2.5% (w/v) phenol and 5% (v/v) water for 2.5 h. The crude peptides were precipitated with ice-cold diethyl ether, recovered by centrifugation and freeze-dried prior to purification with preparative reversed-phase HPLC (see Supporting Information). The purity of the resulting products was confirmed by analytical HPLC, and all peptides were identified by high-resolution ESI-ToF-MS (see the Supporting Information).

Circular dichroism (CD) measurements: CD spectroscopy was carried out on a Jasco J-810 spectropolarimeter (JASCO Deutschland GmbH) equipped with a Jasco PTC-423S Peltier temperature control system and a HAAKE WKL water recirculator (Thermo Electron GmbH) for tempering the samples. Data were collected at 37 °C in a 1.0 mm Quartz Suprasil® cuvette (Hellma Analytics) equipped with a stopper. The overall peptide concentration was 20 μM, and 10 μM in each monomer in the C31/T21 mixtures in 50 mM sodium phosphate buffer supplemented with 150 mM NaCl (pH 7.4). The samples were incubated at 37 °C for 30 min using a thermoshaker (300 rpm) before measuring. CD spectra were recorded in the far-UV range (195–240 nm) at 0.2 nm intervals, 2 nm bandwidth, and 2 s response time with the nitrogen flow rate set to 3.0 L/min and background-corrected by subtraction of the corresponding buffer spectra. The ellipticity was normalized by concentration, number of residues and path length, and the helical content was calculated from the molar ellipticity at 222 nm (see Supporting Information). Thermal denaturation experiments were performed by monitoring the ellipticity change at 222 nm from 25 to 100 °C at a heating rate of 3 °C min^{-1} with 0.1 °C intervals, 1 nm bandwidth, and 1 s response time. The melting temperature T_M was determined as described before.[41] Each reported CD value represents the mean ± SD of three independent measurements. Data analysis occurred with the Spectra Manager™ J-700 software (JASCO Inc). The processing and depiction of the spectra were carried out with the programs Microsoft® Excel Version 16.13 (Microsoft) and OriginPro 2018b version 9.55 (OriginLab Corporation).

Isothermal titration calorimetry (ITC): ITC assay was performed using a MicroCal iTC200 isothermal titration calorimeter (Malvern Panalytical Ltd.). The C31 peptide (100 μM) was injected into the cell containing T21 (10 μM), both in 50 mM sodium phosphate with 150 mM NaCl buffer (pH 7.4). Measurements were conducted at 25 °C, the stirring speed was 750 rpm and the reference power was set to 5 μcal s^{-1}. The total number of injections was 20 with an initial delay of 180 s. For each injection, the filter period was set to 5 s and the spacing between the individual injections was 180 s. For the first injection, 0.5 μL of C31 peptide were injected over a duration of 1.0 s. For injections 2–20, each 2.0 μL of the C31 peptide were added over a time period of 4.0 s. The reference cell contained Milli-Q-H_2O. Before the measurement, the peptide samples were dialyzed against the buffer for 3 h using the Pur-A-Lyzer™ Midi Dialysis Kit (MWCO 1 kDa, Sigma-Aldrich®/Merck KGaA). Data analysis and depiction occurred with the MicroCal LLC ITC200 AddOn for the Origin software 7.0 SP4 (Malvern Panalytical Ltd, OriginLab Corporation). Integration and fitting occurred using the one-set of sites model, in which all the binding sites are considered to be identical. Experiments were repeated twice.

Size exclusion/multi angle light scattering: The oligomerization state of the different C31/T21 assemblies was determined by

applying size exclusion chromatography (SEC) in combination with multi-angle light scattering (MALS). Measurements were carried out at Wyatt Technology Europe GmbH (see the Supporting Information).

HIV infection assay: For generation of viral stocks, CEMx174 cells[42] were infected with HIV-1_{NL4-3} resulting from transfection of HIV-$1_{pBRNL4-3}$,[43] as described previously.[44] At peak of virus replication, supernatants were harvested, filtered through 0.22 μm pore sizes, and stored in aliquots at −80 °C. Respective dilutions of the peptides were incubated with this viral stock for 1 h prior to infection of CEMx174 SEAP cells. Three days p.i., cell culture supernatants were removed and analyzed for SEAP activity using the Phospha-Light™ system (Thermo Fisher Scientific) with VICTOR^3 1420 Multilabel Plate Reader (Perkin Elmer). Values were corrected for background values obtained from uninfected cells and expressed as percent inhibition compared to cells infected in the absence of peptide. Data represent mean values of two independently performed experiments. IC_{50} values were generated using a non-linear fit (dose-response curve with variable hill slope, four parameters) using the program OriginPro 2018b version 9.55 (OriginLab Corporation). Peptide solutions used for inhibition were diluted from 5 mM stock solutions in DMSO.

Crystallization and Structure Determination: An equal amount (1:1 molar ratio) of T21 and C31 or the fluorinated analogues was dissolved in 10 mM Tris buffer containing 100 mM NaCl (pH 8.0) to give an overall concentration of ~10 mg mL^{-1}. The mixture was incubated at 37 °C for 30 min to allow for the formation of the helical bundles. Initial crystallization conditions for the peptide complexes were identified by sparse matrix screening using commercially available screens from Jena Bioscience. Crystallization drops were set up by mixing equal volumes (0.2 μL) of the peptide mixture and reservoir solution in a sitting-drop vapor diffusion system at 19 °C using an Oryx pipetting robot system (Douglas Instruments Ltd.). If necessary, crystallization conditions were refined and reproduced in 48-well sitting drop format, mixing equal volumes of peptide solution with reservoir to reach a total drop volume of 1 μl. Crystals were harvested using a nylon fiber loop, immediately frozen in liquid nitrogen and stored in liquid nitrogen until data collection. Data have been collected at the HZB Berlin using beamline 14.1. For data procession, model building and refinement see Supporting Information. The final model and data were deposited in the Protein Data Bank under the accession codes 6TVQ (C31/T21), 6TVU (C31-DfeGly/T21) and 6TVW (C31-5^3-F_3Ile/T21).

Supporting Information: Materials, names, sequences, characterization, and identification of synthesized peptides. Details on solid-phase peptide synthesis and purification, size exclusion chromatography, multi-angle light scattering analysis, circular dichroism analysis, cell line and crystal structure analysis.

Author Contributions

S.H. performed peptide synthesis, CD, ITC, SEC/MALS experiments and analyzed data. E.N. designed the peptide sequence. C.R. conducted crystal structure analysis. J.M. performed SEC/MALS measurements. A.R., B.S., and J.E. were responsible for biological activity studies. S.H., C.R. and B.K. wrote the paper with input from all authors. B.K. conceived the project and obtained the funding.

Acknowledgements

We thank Professor Dr. Markus Wahl for the generous use of his ITC instrument. We also thank Nicole Holton for her assistance with ITC experiments. We gratefully acknowledge Wyatt Technology Europe GmbH for supporting SEC/MALS measurements. We thank R.C. Desrosiers and R.E. Means for the generous contribution of CEMx174 SEAP reporter cells, Frank Kirchhoff for providing HIV-1_{NL4-3}, and André Gessner, Regensburg, for continuous support. S.H. and B.K. thank the DFG for support in the context of the CRC 1349 "Fluorine-Specific Interactions: Fundamentals and Functions" (project iD 387284271) and the RTG 1582 "Fluorine as Key Element". C.R. acknowledges the Max Planck Society for funding. The diffraction experiments have been carried out at beamline BL 14.1 of the Joint Berlin MX–Laboratory at BESSYII. The authors thank the beamline staff at the MX beamlines at the HZB Berlin for support during data collection. We thank Dr. Allison Ann Berger for proofreading of the manuscript. Open Access funding enabled and organized by Projekt DEAL.

Conflict of Interest

The authors declare no conflict of interest.

Keywords: fluorinated amino acids · gp41 · medicinal chemistry · protein engineering · protein-protein interactions

[1] a) D. C. Chan, D. Fass, J. M. Berger, P. S. Kim, *Cell* **1997**, *89*, 263–273; b) J. A. Esté, A. Telenti, *Lancet* **2007**, *370*, 81–88; c) A. Falkenhagen, S. Joshi, *Mol. Ther. Nucleic Acids* **2018**, *13*, 347–364.
[2] a) D. C. Chan, P. S. Kim, *Cell* **1998**, *93*, 681–684; b) F. Naider, J. Anglister, *Curr. Opin. Struct. Biol.* **2009**, *19*, 473–482; c) I. Steffen, S. Pöhlmann, *Curr. Pharm. Des.* **2010**, *16*, 1143–1158; d) J. Pu, Q. Wang, W. Xu, L. Lu, S. Jiang, *Viruses* **2019**, *11*, 705.
[3] a) A. Lazzarin, *Expert Opin. Pharmacother.* **2005**, *6*, 453–464; b) Y. He, J. Cheng, H. Lu, J. Li, J. Hu, Z. Qi, Z. Liu, S. Jiang, Q. Dai, *Proc. Natl. Acad. Sci. USA* **2008**, *105*, 16332–16337.
[4] a) K. Fosgerau, T. Hoffmann, *Drug Discovery Today* **2015**, *20*, 122–128; b) A. Henninot, J. C. Collins, J. M. Nuss, *J. Med. Chem.* **2018**, *61*, 1382–1414.
[5] M. J. Gomara, I. Haro, *Curr. Med. Chem.* **2014**, *21*, 1188–1200.
[6] B. Berkhout, D. Eggink, R. W. Sanders, *Curr. Opin. Virol.* **2012**, *2*, 50–59.
[7] a) T. Naito, K. Izumi, E. Kodama, Y. Sakagami, K. Kajiwara, H. Nishikawa, K. Watanabe, S. G. Sarafianos, S. Oishi, N. Fujii, *Antimicrob. Agents Chemother.* **2009**, *53*, 1013–1018; b) X. Yao, H. Chong, C. Zhang, S. Waltersperger, M. Wang, S. Cui, Y. He, *J. Biol. Chem.* **2012**, *287*, 6788–6796; c) S. Xiong, P. Borrego, X. Ding, Y. Zhu, A. Martins, H. Chong, N. Taveira, Y. He, *J. Virol.* **2017**, *91*, e01839–01816.
[8] a) F. Gaston, C. Granados Giovana, S. Madurga, F. Rabanal, F. Lakhdar-Ghazal, E. Giralt, E. Bahraoui, *ChemMedChem* **2009**, *4*, 570–581; b) B. D. Welch, J. N. Francis, J. S. Redman, S. Paul, M. T. Weinstock, J. D. Reeves, Y. S. Lie, F. G. Whitby, D. M. Eckert, C. P. Hill, M. J. Root, M. S. Kay, *J. Virol.* **2010**, *84*, 11235–11244.
[9] a) G. H. Bird, N. Madani, A. F. Perry, A. M. Princiotto, J. G. Supko, X. He, E. Gavathiotis, J. G. Sodroski, L. D. Walensky, *Proc. Natl. Acad. Sci. USA* **2010**, *107*, 14093–14098; b) Y. Guo, P.-P. Zhou, S.-Y. Zhang, X.-W. Fan, Y.-W. Dou, X.-L. Shi, *MedChemComm* **2018**, *9*, 1226–1231; c) O. Bolarinwa, M. Zhang, E. Mulry, M. Lu, J. Cai, *Org. Biomol. Chem.* **2018**, *16*, 7878–7882.
[10] D. Wang, M. Lu, P. S. Arora, *Angew. Chem. Int. Ed.* **2008**, *47*, 1879–1882; *Angew. Chem.* **2008**, *120*, 1905–1908.
[11] a) J. T. Ernst, O. Kutzki, A. K. Debnath, S. Jiang, H. Lu, A. D. Hamilton, *Angew. Chem. Int. Ed.* **2002**, *41*, 278–281; *Angew. Chem.* **2002**, *114*, 288–

291; b) A. D. Bautista, O. M. Stephens, L. Wang, R. A. Domaoal, K. S. Anderson, A. Schepartz, *Bioorg. Med. Chem. Lett.* **2009**, *19*, 3736–3738; c) W. S. Horne, L. M. Johnson, T. J. Ketas, P. J. Klasse, M. Lu, J. P. Moore, S. H. Gellman, *Proc. Natl. Acad. Sci. USA* **2009**, *106*, 14751–14756.
[12] a) W.-G. Forssmann, Y.-H. The, M. Stoll, K. Adermann, U. Albrecht, H.-C. Tillmann, K. Barlos, A. Busmann, A. Canales-Mayordomo, G. Giménez-Gallego, J. Hirsch, J. Jiménez-Barbero, D. Meyer-Olson, J. Münch, J. Pérez-Castells, L. Ständker, F. Kirchhoff, R. E. Schmidt, *Sci. Transl. Med.* **2010**, *2*, 63re63; b) M. K. Lee, H. K. Kim, T. Y. Lee, K.-S. Hahm, K. L. Kim, *Exp. Mol. Med.* **2006**, *38*, 18–26.
[13] a) M. T. Augusto, A. Hollmann, M. A. R. B. Castanho, M. Porotto, A. Pessi, N. C. Santos, *J. Antimicrob. Chemother.* **2014**, *69*, 1286–1297; b) C. Wang, S. Xia, X. Wang, Y. Li, H. Wang, R. Xiang, Q. Jiang, Q. Lan, R. Liang, Q. Li, S. Huo, L. Lu, Q. Wang, F. Yu, K. Liu, S. Jiang, *J. Med. Chem.* **2021**, https://doi.org/10.1021/acs.jmedchem.1c00258.
[14] M. Ferrer, T. M. Kapoor, T. Strassmaier, W. Weissenhorn, J. J. Skehel, D. Oprian, S. L. Schreiber, D. C. Wiley, S. C. Harrison, *Nat. Struct. Biol.* **1999**, *6*, 953–960.
[15] a) H. Chong, X. Wu, Y. Su, Y. He, *AIDS* **2016**, *30*, 1187–1196; b) X. Ding, X. Zhang, H. Chong, Y. Zhu, H. Wei, X. Wu, J. He, X. Wang, Y. He, *J. Virol.* **2017**, *91*, e00831–00817; c) S. Su, G. Rasquinha, L. Du, Q. Wang, W. Xu, W. Li, L. Lu, S. Jiang, *Molecules* **2019**, *24*, 1134; d) Y. Zhu, H. Chong, D. Yu, Y. Guo, Y. Zhou, Y. He, V. Simon, *J. Virol.* **2019**, *93*, e02312–02318.
[16] C. Wang, S. Cheng, Y. Zhang, Y. Ding, H. Chong, H. Xing, S. Jiang, X. Li, L. Ma, *Viruses* **2019**, *11*, 811.
[17] a) X. Tang, H. Jin, Y. Chen, L. Li, Y. Zhu, H. Chong, Y. He, F. Kirchhoff, *J. Virol.* **2019**, *93*, e01177–01119; b) M. J. Gomara, Y. Perez, J. P. Martinez, R. Barnadas-Rodriguez, A. Schultz, H. von Briesen, A. Peralvarez-Marin, A. Meyerhans, I. Haro, *Sci. Rep.* **2019**, *9*, 3257; c) D. Wensel, Y. Sun, J. Davis, Z. Li, S. Zhang, T. McDonagh, D. Langley, T. Mitchell, S. Tabruyn, P. Nef, M. Cockett, M. Krystal, V. Simon, *J. Virol.* **2019**, *93*, e00907–00919.
[18] S. Purser, P. R. Moore, S. Swallow, V. Gouverneur, *Chem. Soc. Rev.* **2008**, *37*, 320–330.
[19] a) J. Moschner, V. Stulberg, R. Fernandes, S. Huhmann, J. Leppkes, B. Koksch, *Chem. Rev.* **2019**, *119*, 10718–10801; b) J. Leppkes, T. Hohmann, B. Koksch, *J. Fluorine Chem.* **2020**, *232*, 109453.
[20] H. Mei, J. Han, K. D. Klika, K. Izawa, T. Sato, N. A. Meanwell, V. A. Soloshonok, *Eur. J. Med. Chem.* **2020**, *186*, 111826.
[21] a) G. Akcay, K. Kumar, *J. Fluorine Chem.* **2009**, *130*, 1178–1182; b) M. Salwiczek, E. K. Nyakatura, U. I. M. Gerling, S. Ye, B. Koksch, *Chem. Soc. Rev.* **2012**, *41*, 2135–2171; c) E. N. G. Marsh, *Acc. Chem. Res.* **2014**, *47*, 2878–2886; d) A. A. Berger, J.-S. Völler, N. Budisa, B. Koksch, *Acc. Chem. Res.* **2017**, *50*, 2093–2103; e) S. Huhmann, B. Koksch, *Eur. J. Org. Chem.* **2018**, 3667–3679; f) R. Smits, B. Koksch, *Curr. Top. Med. Chem.* **2006**, *6*, 1483–1498.
[22] D. M. Eckert, P. S. Kim, *Annu. Rev. Biochem.* **2001**, *70*, 777–810.
[23] L. M. Johnson, W. S. Horne, S. H. Gellman, *J. Am. Chem. Soc.* **2011**, *133*, 10038–10041.
[24] a) S. Wang, J. York, W. Shu, M. O. Stoller, J. H. Nunberg, M. Lu, *Biochemistry* **2002**, *41*, 7283–7292; b) D. C. Chan, C. T. Chutkowski, P. S. Kim, *Proc. Natl. Acad. Sci. USA* **1998**, *95*, 15613–15617.
[25] a) S. Jiang, A. K. Debnath, *Biochem. Biophys. Res. Commun.* **2000**, *270*, 153–157; b) Y. He, S. Liu, J. Li, H. Lu, Z. Qi, Z. Liu, A. K. Debnath, S. Jiang, *J. Virol.* **2008**, *82*, 11129–11139.
[26] Y. He, J. Cheng, J. Li, Z. Qi, H. Lu, M. Dong, S. Jiang, Q. Dai, *J. Virol.* **2008**, *82*, 6349–6358.
[27] H. Chong, X. Yao, Z. Qiu, B. Qin, R. Han, S. Waltersperger, M. Wang, S. Cui, Y. He, *J. Biol. Chem.* **2012**, *287*, 20281–20289.
[28] a) H. Chong, X. Yao, J. Sun, Z. Qiu, M. Zhang, S. Waltersperger, M. Wang, S. Cui, Y. He, *J. Biol. Chem.* **2012**, *287*, 34558–34568; b) H. Chong, X. Yao, Z. Qiu, J. Sun, M. Zhang, S. Waltersperger, M. Wang, S.-L. Liu, S. Cui, Y. He, *FASEB J.* **2013**, *27*, 1203–1213.
[29] a) L. T. Rimsky, D. C. Shugars, T. J. Matthews, *J. Virol.* **1998**, *72*, 986–993; b) M. L. Greenberg, N. Cammack, *J. Antimicrob. Chemother.* **2004**, *54*, 333–340.
[30] H. Zheng, K. Comeforo, J. Gao, *J. Am. Chem. Soc.* **2008**, *131*, 18–19.
[31] a) A. Otaka, M. Nakamura, D. Nameki, E. Kodama, S. Uchiyama, S. Nakamura, H. Nakano, H. Tamamura, Y. Kobayashi, M. Matsuoka, N. Fujii, *Angew. Chem. Int. Ed.* **2002**, *41*, 2937–2940; *Angew. Chem.* **2002**, *114*, 3061–3064; b) H. Nishikawa, S. Nakamura, E. Kodama, S. Ito, K. Kajiwara, K. Izumi, Y. Sakagami, S. Oishi, T. Ohkubo, Y. Kobayashi, A. Otaka, N. Fujii, M. Matsuoka, *Int. J. Biochem. Cell Biol.* **2009**, *41*, 891–899.
[32] a) H.-P. Chiu, Y. Suzuki, D. Gullickson, R. Ahmad, B. Kokona, R. Fairman, R. P. Cheng, *J. Am. Chem. Soc.* **2006**, *128*, 15556–15557; b) H. Erdbrink, E. K. Nyakatura, S. Huhmann, U. I. M. Gerling, D. Lentz, B. Koksch, C. Czekelius, *Beilstein J. Org. Chem.* **2013**, *9*, 2009–2014; c) U. I. M. Gerling, M. Salwiczek, C. D. Cadicamo, H. Erdbrink, C. Czekelius, S. L. Grage, P. Wadhwani, A. S. Ulrich, M. Behrends, G. Haufe, B. Koksch, *Chem. Sci.* **2014**, *5*, 819–830.
[33] S. Huhmann, E. K. Nyakatura, H. Erdbrink, U. I. M. Gerling, C. Czekelius, B. Koksch, *J. Fluorine Chem.* **2015**, *175*, 32–35.
[34] Y. H. Zhao, M. H. Abraham, A. M. Zissimos, *J. Org. Chem.* **2003**, *68*, 7368–7373.
[35] P. Setny, R. Baron, J. A. McCammon, *J. Chem. Theory Comput.* **2010**, *6*, 2866–2871.
[36] L. Shen, S. Peterson, A. R. Sedaghat, M. A. McMahon, M. Callender, H. Zhang, Y. Zhou, E. Pitt, K. S. Anderson, E. P. Acosta, R. F. Siliciano, *Nat. Med.* **2008**, *14*, 762–766.
[37] a) A. Ashkenazi, Y. Wexler-Cohen, Y. Shai, *Biochim. Biophys. Acta Biomembr.* **2011**, *1808*, 2352–2358; b) Y. Zhu, X. Ding, D. Yu, H. Chong, Y. He, V. Simon, *J. Virol.* **2020**, *94*, e01358–01319.
[38] E. Krissinel, K. Henrick, *J. Mol. Biol.* **2007**, *372*, 774–797.
[39] X. Yao, H. Chong, C. Zhang, Z. Qiu, B. Qin, R. Han, S. Waltersperger, M. Wang, Y. He, S. Cui, *J. Biol. Chem.* **2012**, *287*, 26618–26629.
[40] G. B. Fields, R. L. Noble, *Int. J. Pept. Protein Res.* **1990**, *35*, 161–214.
[41] M. Salwiczek, S. Samsonov, T. Vagt, E. Nyakatura, E. Fleige, J. Numata, H. Cölfen, M. T. Pisabarro, B. Koksch, *Chem. Eur. J.* **2009**, *15*, 7628–7636.
[42] R. D. Salter, D. N. Howell, P. Cresswell, *Immunogenetics* **1985**, *21*, 235–246.
[43] S. Carl, R. Daniels, A. J. Iafrate, P. Easterbrook, T. C. Greenough, J. Skowronski, F. Kirchhoff, *J. Infect. Dis.* **2000**, *181*, 132–140.
[44] C. Haußner, D. Damm, S. Nirschl, A. Rohrhofer, B. Schmidt, J. Eichler, *ChemBioChem* **2017**, *18*, 647–653.

Manuscript received: August 14, 2021
Revised manuscript received: October 4, 2021
Accepted manuscript online: October 4, 2021
Version of record online: October 22, 2021